Asia-Pacific J. Atmos. Sci., 48(3), 227-241, 2012
DOI:10.1007/s13143-012-0023-5

Simulation of Urban Climate with High-Resolution WRF Model: A Case Study in Nanjing, China

Ben Yang[1], Yaocun Zhang[1], and Yun Qian[2]

[1]*School of Atmospheric Sciences, Nanjing University, Nanjing, China*
[2]*Pacific Northwest National Laboratory, Richland, U. S. A.*

(Manuscript received 21 April 2011; revised 15 December 2011; accepted 24 February 2012)

Abstract: In this study, urban climate in Nanjing of eastern China is simulated using 1-km resolution Weather Research and Forecasting (WRF) model coupled with a single-layer Urban Canopy Model. Based on the 10-summer simulation results from 2000 to 2009 we find that the WRF model is capable of capturing the high-resolution features of urban climate over Nanjing area. Although WRF underestimates the total precipitation amount, the model performs well in simulating the surface air temperature, relative humidity, and precipitation frequency and inter-annual variability. We find that extremely hot events occur most frequently in urban area, with daily maximum (minimum) temperature exceeding 36°C (28°C) in around 40% (32%) of days. Urban Heat Island (UHI) effect at surface is more evident during nighttime than daytime, with 20% of cases the UHI intensity above 2.5°C at night. However, The UHI affects the vertical structure of Planet Boundary Layer (PBL) more deeply during daytime than nighttime. Net gain for latent heat and net radiation is larger over urban than rural surface during daytime. Correspondingly, net loss of sensible heat and ground heat are larger over urban surface resulting from warmer urban skin. Because of different diurnal characteristics of urban-rural differences in the latent heat, ground heat and other energy fluxes, the near surface UHI intensity exhibits a very complex diurnal feature. UHI effect is stronger in days with less cloud or lower wind speed. Model results reveal a larger precipitation frequency over urban area, mainly contributed by the light rain events (< 10 mm d^{-1}). Consistent with satellite dataset, around 10-20% more precipitation occurs in urban than rural area at afternoon induced by more unstable urban PBL, which induces a strong vertical atmospheric mixing and upward moisture transport. A significant enhancement of precipitation is found in the downwind region of urban in our simulations in the afternoon.

Key words: WRF, urban climate simulation, temperature, precipitation, urban planet boundary layer

1. Introduction

Urbanization, one of the extreme cases of land-use change, plays an important role in modifying the surface and low-layer atmospheric properties (Clarke, 1969; Uno *et al.*, 1988; Coutts *et al*., 2007; Ren *et al.*, 2008; Roy and Yuan, 2009). With a large scale of immigrations of population from rural to urban areas the population in cities has been growing at a much faster rate than the earth's total population. The scale and density of cities are expected to rapidly increase in the near future (World Resources Institute, 1996).

The moisture availability and thermal property, associated with the impervious materials and infrastructures geometry (e.g., buildings, streets, and highways) at artificial surfaces, are potentially favorable for solar energy storage in urban areas (Oke, 1981, 1982), resulting in a warmer microclimate regime compared with surrounding rural areas. In addition, Anthropogenic Heat (AH) produced by expanded human activities enhances the warming effect. The warmer urban condition, which is called Urban Heat Island (UHI), typically occurs under clear skies with weak ambient wind (Bornstein, 1968; Clarke, 1969; Shreffler, 1978). Early studies found that the UHI effect can induce a modification of cloudiness and precipitation around urban area (Khemani and Ramana Murty, 1973; Changnon *et al*., 1976; Braham, 1979; Inoue and Kimura, 2004). It is often found that the maximum precipitation is located at downwind of urban area. Burian and Shepherd (2005) found that the urban and its downwind region received more precipitation from noon to midnight by 59% and 30%, respectively, than upwind region in Houston. Mote *et al*. (2007) analyzed the radar signature of precipitation distribution modified by urban and found that the precipitation in eastern metropolitan Atlanta (up to 80 km east to downtown Atlanta) is 30% larger than the western region of the city as westerly prevails.

Numerical models are useful tools in meteorological research because of its ability in providing more detailed 3-dimensional fields and its convenience in doing sensitivity experiments to explore the fundamental mechanism of weather and climate change. Recently, single-layer or multi-layer Urban Canopy Models (UCM) are developed and coupled with mesoscale atmospheric models (Masson, 2000; Kusaka *et al*., 2001; Thanh Ca *et al*., 2002; Kusaka and Kimura, 2004a; Chin *et al.*, 2005; Holt and Pullen, 2007; Miao *et al*., 2009). A recent intercomparison project with 32-member of UCMs, which aimed to understand the complexity required to model energy and water exchanges in urban area, showed that there are a large range of differences in simulated urban surface energy fluxes when using different UCMs (Grimmond *et al.*,

Corresponding Author: Ben Yang, School of Atmospheric Sciences, Nanjing University, 22 Hankou Road, Nanjing, Jiangsu 210093, P. R. China.
E-mail: brady1234.student@gmail.com

2010, 2011). Based on different statistical measures, their results suggested that no models perform best or worst for all fluxes and the simpler models can perform as well as the more complex models. Using a single-layer UCM, Kusaka and Kimura (2004b) analyzed the contribution of canopy structure and AH to the formation of UHI. Trusilova e*t al*. (2009) simulated the effects of urban land expansion on temperature and precipitation using the Mesoscale Model Version 5 (MM5) coupled with the Town Energy Budget model. They revealed that the expansion of current European urban area by 40% would lead to an enlargement of regions affected by thermal stress by a factor of 2 and a reduction of 0.2 mm d^{-1} in precipitation in summer due to disturbances of water cycle caused by urban surfaces.

Due to large computational cost of simulations, most of previous modeling studies were restricted to a few weather episodes. However, the intensity of urban effects varies from case to case and is modulated by synoptic weather patterns, especially by cloud cover and wind speed (Martilli, 2002; Kim and Baik, 2005; Shepherd, 2005; Souch and Grimmond, 2006; Shou and Zhang, 2010). A 40-year model simulation with 10-km resolution around Brussels Capital Region was conducted by Hamdi *et al*. (2009). Their results showed that the local temperature change can either be exaggerated or minimized by the effects of large-scale circulations. Based on two sensitivity experiments for a specific precipitation event, Kusaka *et al.* (2009) revealed the precipitation signals induced by urban effect are not reliable over the urban area surrounded by the complex terrain because of the strong chaos influence in precipitation simulation. Then they conducted eight Augusts (2001-2008) simulations to examine the impacts of urbanization of Tokyo on rainfall amount by the 4-km resolution regional climate model and concluded that climate simulation can be applied as a viable and efficient method. Precipitation modification by urban environment varies and the urban effect can be more dominant than agricultural or topographic influences on days with weaker forcing (Hand and Shepherd, 2009). Therefore, lone-term simulations are needed to provide more reliable and comprehensive results to reproduce the urban impact in regional and global climate modeling (Jones *et al.*, 1989; Oleson *et al.*, 2008).

The city of Nanjing, as Capital of Jiangsu Province, is located in the Yangtze River Delta region with a typical East Asian monsoon climate regime, which is the most developed area in China. As a result of economic reform starting at the end of 1970s, Nanjing has experienced significant industrial and economic growth, which causes distinct expansion of urban area and changes of local climate environment. In this study, the Weather Research and Forecasting (WRF) model coupled with a single-layer UCM is used to simulate the local-scale climatic features and urban effect around Nanjing area (Chen and Dudhia, 2001; Chen *et al*., 2006; Skamarock *et al.*, 2008). The effects of different urban underlying surfaces on temperature and precipitation are examined by analyzing the simulation results with fine spatial resolution for 10 summers (June-July-August) from 2000 to 2009.

The paper is organized as follows: section 2 describes the model configuration. The performance of WRF simulation is evaluated in section 3. The impacts of urban surface on temperature and precipitation are discussed in section 4. Conclusion and discussion are given in section 5.

2. Model configuration

The WRF version 3.0 is used in this study. The WRF is a fully compressible and non-hydrostatic model with terrain-following pressure coordinate and Arakawa C-grid. The Yonsei University Planet Boundary Layer (PBL) scheme (Hong *et al*., 2006) is used to represent the PBL and sub-grid scale processes and Single-Moment 3-class scheme (WSM3) (Hong *et al*., 2004; Hong and Lim, 2006) to represent the microphysical processes. For the two outer domains, we use Kain-Fritsch cumulus parameterization scheme (Kain, 2004); while for the inner 1 km-resolution domain the model is run with the explicit convection option. The Sea Surface Temperature (SST) is updated every 6 hr for the outmost domain. Updating SST is important for improving the precipitation simulation resulting from more realistic depiction of wind and moisture flux (Bukovsky and Karoly, 2009).

The Noah Land Surface Model (LSM) (Chen and Dudhia, 2001) is used to link the land-air interaction. Noah LSM can predict skin temperature and moisture, which is important in regional climate simulation because the moisture feedback plays an important role in air-land surface interaction (Bukovsky and Karoly, 2009). To represent the thermal and dynamic effects of urban surfaces, a single-layer UCM (Kusaka *et al*., 2001) is coupled in Noah LSM, which takes urban geometry and AH into account in its surface energy budgets and wind shear calculation. The UCM has three urban categories as follows: 1) *Low Intensity Residential* (LIR), 2) *High Intensity Residential* (HIR), and 3) C*ommercial/Industrial/Transportation* (CIT), which respectively have different construction materials coverage, populations, AH emissions, and so on. AH, being treated as an additional term in the sensible heat flux in the UCM, includes a diurnal cycle with 2 peaks at rush hours around 08 LST and 17 LST, respectively. Same as the default setting in the WRF (Tewari *et al*., 2007), the maximum values of AH at 17 LST are 20, 50 and 90 w m^{-2} over LIR, HIR and CIT area, respectively.

The land-use condition of the innermost domain (Fig. 1b) is derived from the U.S. Geological Survey 30 dataset with 24-category of land surface types (1992). To represent the current land-use feature in Nanjing, an expansion of urban coverage and a conversion from HIR to CIT area at the city downtown are conducted according to the land-use information provided by Bureau of Urban Planning of Nanjing.

Focusing on the city of Nanjing, the simulations are conducted over three-nesting domains with 60 × 60, 60 × 60, and 80 × 80 grid points and 25, 5, and 1-km grid spacing, respectively (Fig. 1a). The vertical grid contains 35 full sigma levels

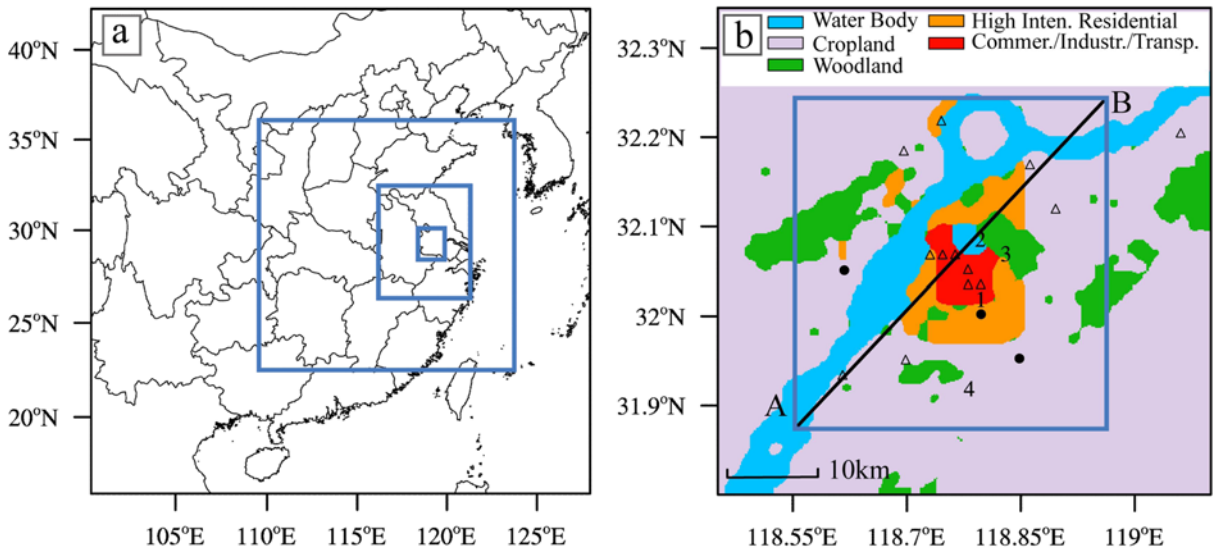

Fig. 1. (a) Three-nesting domains with 25 km, 5 km, and 1 km grid spacing in WRF. (b) Land-use in the inner 1 km resolution domain. Numbers in (b) represent the selected Automatic Meteorology Stations (AMS), e.g., 1 = Guanghua East-Street; 2 = Xuanwu Lake; 3 = Arboretum and 4 = Hehei University and Triangle represent unselected AMS sites. Dots are the locations for China Rain Gauge Stations (RGS). Blue Solid box shows sub-domain used for basic analysis and average. Line AB marks the vertical cross section used in Fig. 6.

from the surface to 50 hPa, of which nearly 10 levels are below 1 km so as to have finer vertical resolution within the PBL. The simulations are carried out for 3 months starting at June 1 and ending at September 1 of each year from 2000 to 2009. Initial and boundary conditions for variables wind, temperature, water vapor, pressure (*U, V, T, Q, P*) *et al.* in the outermost domain are from the National Centers for Environment Prediction (NCEP) operational Global Final (FNL) Analyses data on a $1.0^{o} \times 1.0^{o}$ grid at a 6-hr interval.

3. Model evaluation

The WRF simulations are evaluated against three observational datasets. The first one is Tropical Rainfall Measuring Mission (TRMM) 3B42 datasets (Huffman *et al.*, 2007), with a spatial resolution of 0.25 degree and a temporal resolution of 3 hr. The second one is Rain Gauge Station (RGS) observations for 2000-2007, acquired from National Meteorological Information Center of China Meteorological Administration. The third one is the Automatic Meteorological Station (AMS) data for 2006-2009, acquired from Nanjing Weather Bureau. The locations of observational sites are shown in Fig. 1b. Four AMS sites 1) *Guanghua East-Street*, 2) *Xuanwu Lake*, 3) *Arboretum* and 4) *Hehei University,* representing land-use types of *Urban Area*, *Water Body*, *Wood Land* (WL) and *Crop Land* (CL), respectively, are used in the evaluation.

AMS sites can provide hourly temperature and Relative Humidity (RH) at 2 m height from surface, at which level model outputs are diagnosed by the Monin-Obukhov (M-O) similarity theory. Specific Humidity at 2 m height is also derived by the observed temperature, RH and near surface pressure. Because the water body information in model's inside domain is not updated during the simulation, only three AMS sites (No. 1, 3, and 4) are selected to validate the simulated temperature and humidity. Figure 2 compares the observed and simulated diurnal cycles of mean temperatures, Specific Humidity and RH at 2 m height above the 3 types of land surfaces. The differences between simulation and observation are also shown.

The observation shows that the surface air temperature over three land surface types all reach maximum at around 14-15 LST and minimum at around 06-07 LST, respectively. The observed temperature over CL is 0.5-1.0°C lower than over Urban Area, but 0.5-2.5°C higher than over WL. These diurnal features of temperature and the differences among the 3 land surface types are generally well captured by the model. The observations also reveal the air temperature over WL is much lower than over Urban and CL during night. After sunrise, temperature over WL rises more rapidly than over Urban Area, which decreases the daytime temperature difference between Urban and WL. From Fig. 2g, we can see that the temperature bias is most significant over urban surface but usually less than 2°C. The temperature bias is more evident during daytime than nighttime over CL. A weak negative bias of simulated temperature over WL can be found in the morning but becomes positive after 15 LST.

In the observation (Figs. 2a and 2b), the variations of Specific Humidity and temperature are anti-correlated over urban area and CL at diurnal cycle, with minimum humidity at around 14-15 LST and maximum value at around 08-09 LST. The Specific Humidity over CL is about 0.5 g kg^{-1} larger than over urban area. The diurnal feature of Specific Humidity and its correlation with temperature are well simulated by the model over urban area and CL. The observed Specific Humidity over

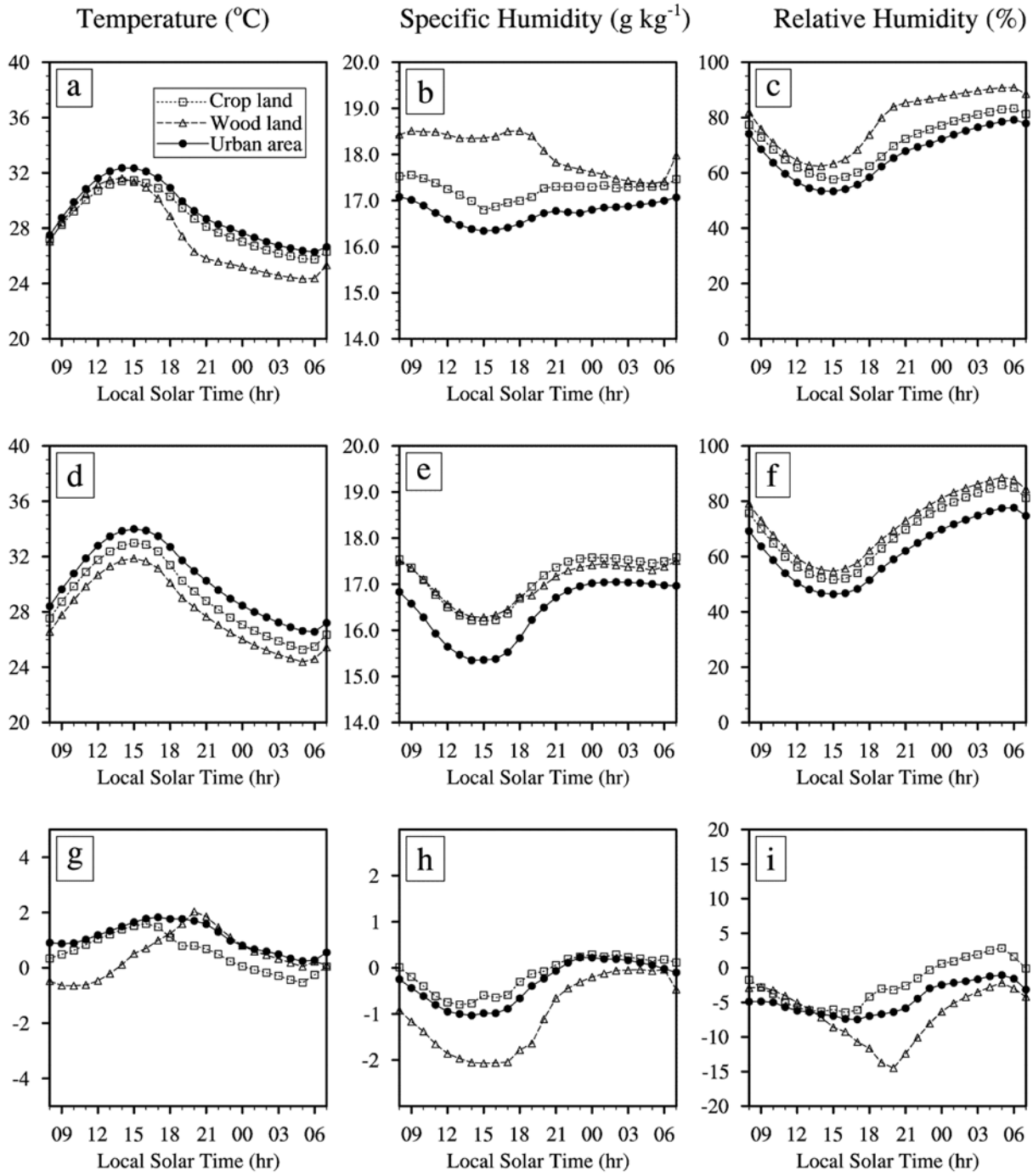

Fig. 2. Diurnal cycles of 2 m height temperature (left), specific humidity (middle) and relative humidity (right) in observations (top), simulations (middle) and their differences (bottom), over different underlying surfaces averaged from 2006 to 2009. Observations over urban area, wood land and crop land are from AMS sites of No. 1 (Guanghua East-Street), No. 3, (Arboretum) and No. 4 (Hehei University), respectively.

WL shows a different diurnal characteristic from over other two land surface types, with a larger value during daytime. Such feature is not captured by the model, probably due to a poor simulation of land-air moisture exchange and vertical moisture transport over WL during daytime. The difference between observed and simulated Specific Humidity is evident during daytime, especially over WL. The variation of observed surface air RH is anti-correlated with temperature at diurnal cycle over all the three land surface types (Figs. 2a and 2c), with minimum RH at around 14-15 LST and maximum RH at around 06-07 LST, respectively. Opposite to temperature, RH over urban area is lower than over other two types of surface due to different temperature condition and moisture availability, which is captured well by WRF simulation. The model biases

for RH is usually less than 15%, with a maximum number over WL at later afternoon.

Daily rainfall data for model evaluation are derived from TRMM, RGS and AMS sites. Because the rainfall data for *Guanghua East-Street* Station is not available, we use observations from the rest of 3 AMS stations, together with observation from TRMM and 3 RGS sites for precipitation evaluation. Hereafter, rainy-day refers to a day with precipitation rate larger than 0.2 mm d^{-1}. The simulated and observed mean precipitation amount and frequency from 2000 to 2009 are shown in Fig. 3. While the inter-annual variability of precipitation amount and frequency are generally captured, model significantly underestimates the rain amount. The precipitation frequency is better simulated, indicating that model may fail to capture the heavy precipitation events. The systematic bias of precipitation amount is probably due to the simplicity of the WSM3 microphysics parameterization scheme, which doesn't include the graupel and may fail to capture heavy precipitation events (Kusaka *et al.*, 2010). Another possible factor resulting in the systematic biases is probably related to the coarse spatial resolution of reanalysis forcing data used in this study. Previous studies based on the hourly RGS data over China found two peaks for summer rainfall diurnal cycle at around 05 LST and 17 LST, respectively, over Yangzi River Delta (Yu *et al*., 2007). Figure 4 shows the WRF simulated diurnal cycle of precipitation averaged over Nanjing, with two peaks at around 07 LST and 20 LST, approximately 2-3 hour later than the RGS values averaged over Yangzi River Delta region. However, a comparison study between rain gauge data and TRMM satellite data revealed that TRMM may not be able to capture the precipitation peak in the early morning over Yangzi River Delta (Zhou *et al.*, 2008), which

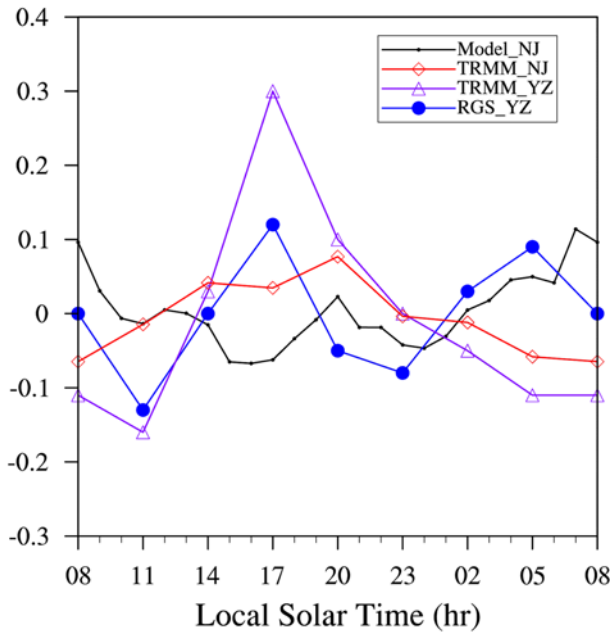

Fig. 4. Diurnal cycles of simulated and observed summer precipitation (subtracted by the diurnal mean, mm hr^{-1}) over Nanjing. The diurnal cycles of observed precipitation from Rain Gauge Station and TRMM over Yangzi River Delta region for 2000 to 2004 (adapted from Zhou *et al.,* 2008) are also presented.

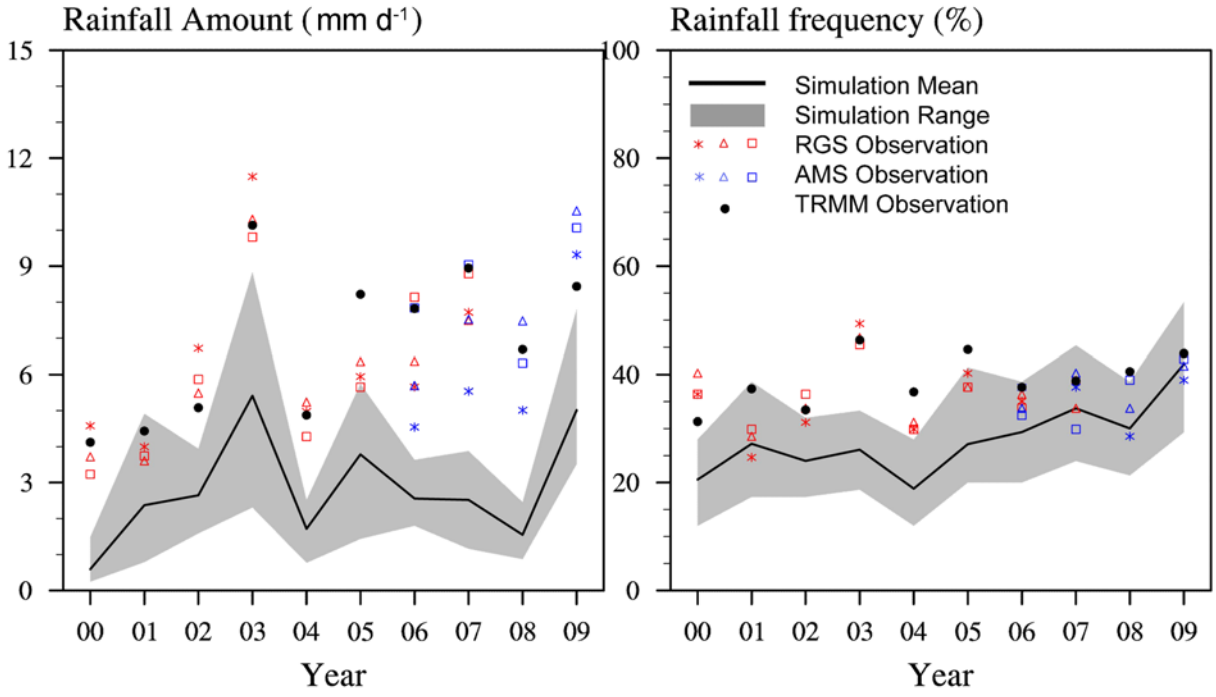

Fig. 3. Inter-annual variations of observed and simulated summer (June 16-August 31) precipitation amount and frequency in Nanjing from 2000 to 2009. Simulation Mean and range respectively denote the average and maximum/minimum of summer precipitation in the sub-domain as defined in Fig. 1b. RGS, AMS and domain-average TRMM Observations are indicated by red, blue and black markers, respectively.

impose more uncertainties in evaluating the diurnal cycle of precipitation. From Fig. 4, we can find that the peak time of TRMM precipitation averaged over Nanjing is about 2-3 hr later than that averaged over the broad Yangzi River Delta.

Overall, although WRF underestimates the total precipitation amount, the model performs well in simulating the surface air

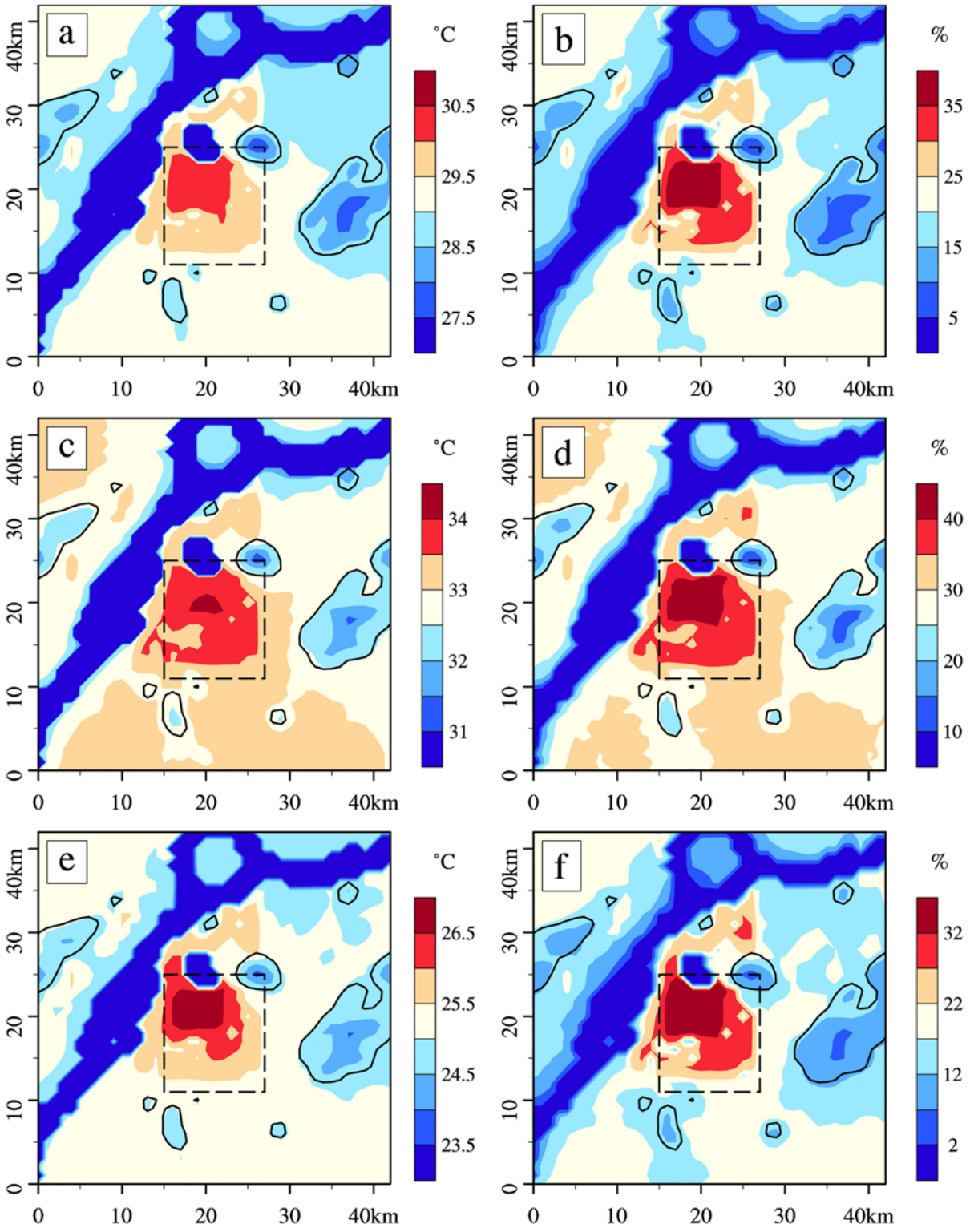

Fig. 5. (Left panel) Simulated spatial distributions of daily (a) mean, (c) maximum, and (e) minimum temperature. (Right panel) Simulated spatial distributions of frequency of hot days with daily (b) mean, (d) maximum, and (f) minimum temperature exceeding 32°C, 36°C, and 28°C, respectively. Black solid lines and dashed lines represent mountain and urban areas, respectively.

temperature, RH, and precipitation frequency, and inter-annual variability.

4. Urban impacts on temperature and precipitation

a. Temperature effect

Figure 5 (left panels) shows the spatial distributions of simulated daily mean (Tmean), maximum (Tmax), and minimum (Tmin) temperatures at 2 m height averaged for 10 summers from 2000-2009. A close spatial correlation between temperature and land-cover features (Fig. 1b) can be seen. The commercial district in Nanjing is always hottest, with Tmean, Tmax, and Tmin exceeding 30°C, 34°C and 26.5°C, respectively. Urban area is 1-2°C warmer in both daytime and nighttime than surrounding suburban and rural areas, where mostly are CL or WL, with the Tmean, Tmax and Tmin around 29°C, 33°C and 25°C, respectively.

Figure 5 (right panels) shows the frequency of hot days with Tmean, Tmax, and Tmin larger than 32°C, 36°C and 28°C, respectively. We can find there are around 40% of days during 10-summer simulation period with Tmax above 36°C over the commercial district, while only 25-35% of days are over CL or WL. Hot night condition also occurs most frequently in the urban area, i.e., around 32% of days with Tmin above 28°C over commercial district and less than 22% of days over other regions.

To look at how atmospheric properties within PBL are affected by the underlying surface, Fig. 6 presents the vertical profiles of mean potential temperatures during daytime (10-17 LST) and nighttime (20-03 LST) along a cross section depicted in Fig. 1b. During daytime, the potential temperature over urban surface is higher than over surrounding area. Such difference is most significant at near surface, and becomes less evident with increasing altitude. Different low layer atmospheric stability can also be seen over different land surface types. There is an unstable layer below 200 m height over urban surface, while the atmosphere shows a more stable environment over surrounding area. A more evident stable low-layer atmosphere can be seen over water surface. At night, potential temperature (as well as temperature, not shown) is mainly controlled by the large scale meteorology field. The atmosphere is very stable except for a weak unstable layer below 100 m over urban surface.

Figure 6c shows the vertical distribution of UHI intensity (UHII), defined as temperature difference between urban area (Commercial area, referred as CA) and rural area (CL and WL, referred as CW) in the sub-domain (Fig. 1b), for both daytime and nighttime average. It is found that during daytime the UHII is around 0.5°C near surface then gradually decrease vertically to about 1200 m height. Near surface UHI during nighttime is stronger than during daytime, with an intensity of about 0.7°C. The UHII, however, decreases vertically with height more rapidly during nighttime than daytime because of thicker PBL in daytime.

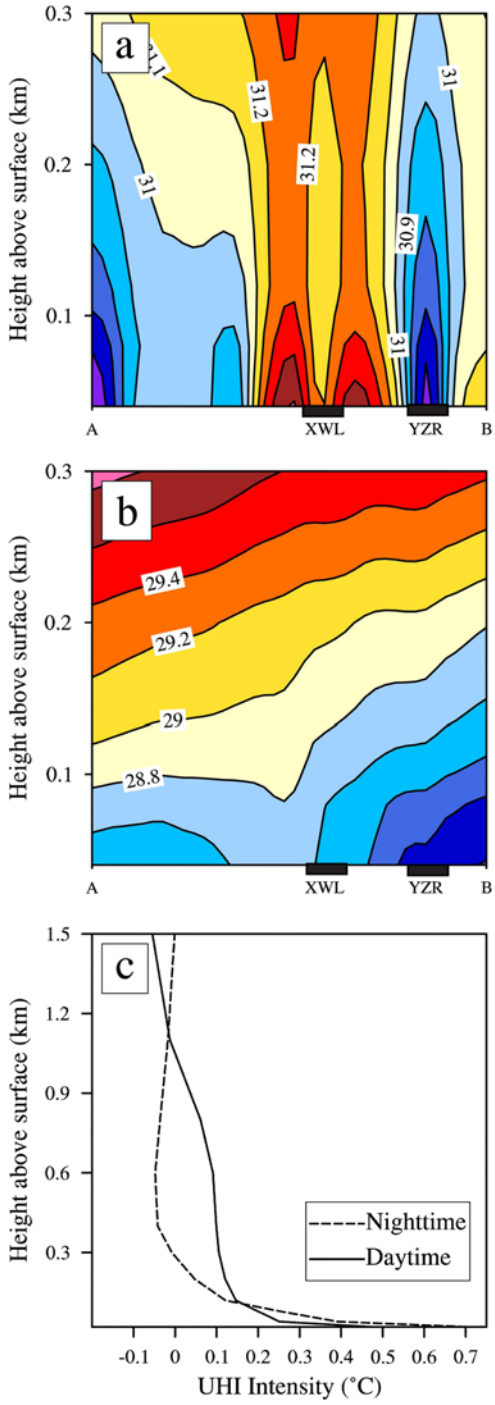

Fig. 6. Simulated cross sections (AB in Fig. 1b) of potential temperature (°C) for (a) daytime (10-17 LST) and (b) nighttime (20-03 LST) average; (c) Simulated vertical distributions of Urban Heat Island (UHI) intensity for daytime and nighttime average. XWL: Xuanwu Lake; YZR: Yangtze River. UHI intensity is defined as temperature difference between urban (commercial area) and rural area (cropland and woodland) in the sub-domain in Fig. 1b.

UHI effect is mainly caused by the distinguished moisture availability and thermal properties associated with the impervious materials and infrastructures geometry at artificial surface. Additional AH also contributes to the UHI. To analyze

how the energy budgets over different underlying surfaces affect the UHI, Figure 7 exhibits the diurnal cycles of UHII and the differences of surface energy fluxes, including sensible heat (SH), latent heat (LH), ground heat (GH) and net radiation (NR, shortwave + longwave), between urban (i.e. CA) and rural (i.e., CW) surfaces. Positive difference for energy flux means more net energy gain at urban surface than rural surface. Figure 7b also shows the UHII (normalized by daily mean and variance) at surface, 2 m height and upper-layer in PBL (100-1000 m height). It should be noted that only results from non-rainy days are used in these plots since surface energy features alter significantly when it rains (discussed later).

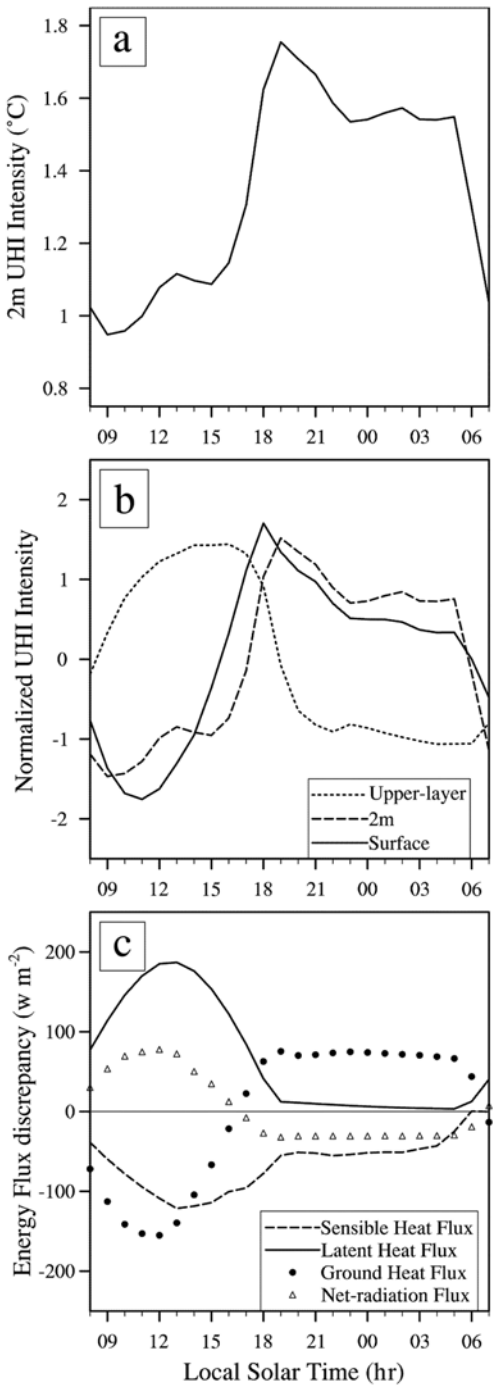

Fig. 7. Simulated diurnal cycles of (a) 2 m height UHI intensity, (b) different levels' UHI intensities and (c) urban and rural energy flux differences, on non-rainy days. Urban area includes commercial area and rural area includes cropland and woodland inside the sub-domain in Fig. 1b. In (b) the values are normalized by daily mean and variance, and upper-layer means 100-1000 m height.

Figure 7a shows that most intense UHI effect at 2 m height occurs at 19 LST, with UHII around 1.7°C, while the weakest UHII (0.9°C) occurs at 09 LST. On average, daytime UHI is much weaker than nighttime at 2 m height, which is consistent with Fig. 6c. Huang *et al.* (2007) found that near surface UHI during nighttime is stronger than during daytime in Nanjing, with a strong and stable UHI during 00 to 05 LSL. They also revealed that the diurnal cycle of UHII in Nanjing has two peaks at around 20 and 02 LST, respectively. Therefore, the diurnal cycle of UHII in Nanjing is reasonably captured by the model in this study. By comparing Fig. 7b with Fig. 7c, we can find a close correlation for diurnal cycles between UHII and energy budgets at surface. Surface UHII decreases after sunrise and reaches a minimum value at around 11 LST. Then it starts to increase from 11 LST and reaches its maximum at 18 LST. Figure 7c shows that the NR is larger over urban than rural area during daytime, indicating urban surface gains more radiation than rural area. Meanwhile LH gain is also larger over urban area probably because of less evaporation over urban surface. Correspondingly, the net SH and GH loss at surface are larger over urban area than rural area resulting from warmer skin temperature over the urban surface during daytime.

At higher level within PBL, UHII is stronger during daytime than nighttime. As shown in Fig. 7c, SH difference is larger during daytime, indicating a more active vertical mixing over urban area than rural area. At night, upper-layer UHII becomes much weaker as shown in Fig. 6c. Since the results at 2 m height are derived based on M-O similarity theory, we can find the 2 m UHII is affected by the strong SH flux in the afternoon over urban surface. Generally, the UHII (especially at 2 m height) shows a complex diurnal cycle mainly because of different diurnal characteristics of urban-rural difference in LH, GH and other energy fluxes, i.e., large GH flux at urban surface reduces the UHII after sunrise but favors a stable and strong nighttime UHI; small urban LH significantly enhances the UHI at afternoon. The peak time of AH (around 17-18 LST) and the nighttime warming effect of walls may also contribute to the 2 peaks (19 and 02 LST) of near surface UHII.

The UHII is modulated by synoptic weather patterns and varies from case to case. The frequency distributions of UHII at 2 m height, for both daytime and nighttime average, are given in Fig. 8. We can find that the most frequently-appeared UHII is from 1°C to 2.5°C during daytime, and for about 42% of days in the 10 summers the UHI intensity is around 1.5-2°C. Overall pattern of frequency distribution during nighttime is similar with that during daytime, except for more frequent strong UHI events (larger than 2°C) occurring at night. For example, 20% of frequency presents UHII above 2.5°C during

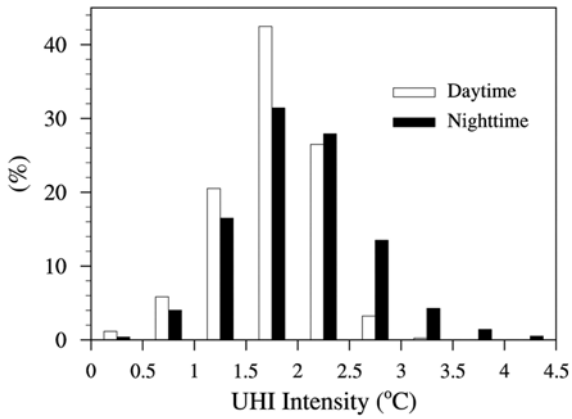

Fig. 8. Simulated frequency of occurrence of UHI intensities at 2 m height for daytime (10-17 LST) and nighttime (20-03 LST) average. UHI intensity is defined same as in Fig. 6.

Table 1. Temperature changes in non-rainy/rainy condition, and in weak/strong wind condition for both daytime (10-17 LST) and nighttime (20-03 LST) average. Here, A = Non-rainy (precipitation rate < 0.2 mm d^{-1}); B = Rainy (precipitation rate > 0.2 mm d^{-1}); C = Weak wind (200 m wind speed < 5 m s^{-1}); D = Strong wind (200 m wind speed > 5 m s^{-1}).

	B-A		D-C	
	Daytime	Nighttime	Daytime	Nighttime
Urban	–3.99	–1.66	–0.41	–0.32
Rural	–4.44	–1.08	–0.74	0.67

nighttime, but only 5% during daytime.

Cloud/precipitation and wind speed are the most important factors that affect UHII. We analyzed the relationships of daily mean UHII at 2 m height with wind speed at 200 m height and cloud amount vertically integrated from 500 to 2000 m. Correlation coefficient between UHII and wind speed is –0.67, indicating a strong UHI effect at lower-wind speed synoptic condition. A negative correlation coefficient of –0.39 is found between UHII and cloud amount, indicating a weaker UHI effect in cloudy or rainy days.

To further analyze how large-scale synoptic systems affect the UHII, surface energy budgets are compared for urban and rural areas in non-rainy/rainy days and weak/strong wind conditions based on daily rainfall and 200 m wind speed, respectively. From Table 1 and Fig. 9 (left) we can find that temperatures decrease in both urban and rural area because of less absorption of solar radiation at rainy days, and the decreases are more evident in daytime. Obviously, urban area experiences a smaller temperature change than rural area during daytime but larger during nighttime at rainy days.

Rainy days are excluded when analyzing the impact of wind-speed on UHII (right panel of Fig. 9). SH and GH fluxes are more sensitive to wind speed at urban surface than rural surface, but LH flux is more sensitive over rural surface. It can be seen that, stronger wind speed significantly increases the SH release to atmosphere at urban surface during daytime, consequently reducing the downward GH flux. The loss of both SH and LH increase under stronger wind condition over rural area because larger wind benefits the sensible heat transfer and evaporation.

b. Precipitation effect

The temporary and spatial distributions of precipitation can be modified by urban underlying features. We classify precipi-

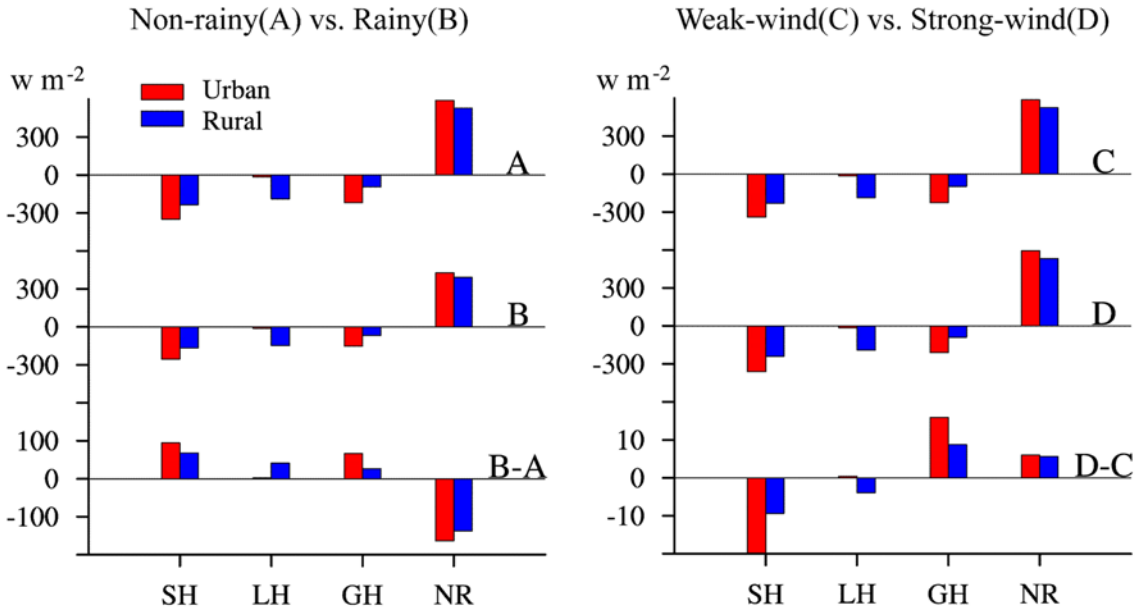

Fig. 9. Simulated energy fluxes in non-rainy vs. rainy conditions (Left panel), and weak vs. strong wind conditions (right panel), for daytime (10-17 LST) average. Urban and rural areas are defined same as in Fig. 7. SH = Sensible Heat Flux; LH = Latent Heat Flux; GH = Ground Heat Flux; NR = Net Radiation flux. Positive values mean net energy gain at surface.

tation events into light, moderate, and heavy ones, with rainfall 0.2-10 mm d^{-1}, 10-25 mm d^{-1} and > 25 mm d^{-1}, respectively. Figure 10 shows the simulated spatial distributions of frequencies for the 3 classes of precipitation events, as well as their total amount. The domain-average frequencies of light, moderate and heavy precipitation in simulation are 19.6%, 2.9% and 4.1%, respectively, while the frequencies derived from TRMM observation are about 19.4%, 8.4% and 9.4%, indicating the model well capture the light rain frequency but underestimate the moderate and heavy rain events. From model results, it is clear that large precipitation frequency, mainly contributed by light rain, can be found over urban area and mountains at the east and west sides of the domain. The averaged precipitation frequency over urban area reaches 27% and 21% for total and light rain events, respectively, which is much larger than entire domain average. The urban impact on moderate and heavy rain events is relatively small.

Figures 11a and 11b show the diurnal cycle of the ratio of urban to rural precipitation (mountain areas not included) from TRMM observation and model results. The diurnal cycle of ratio of precipitation between urban and rural area are well simulated by WRF. It is obvious that both precipitation amount and frequency are larger over urban area than rural area during daytime. High resolution model results show that the urban impact on precipitation is most prominent at 13 LST when precipitation amount (frequency) is around 20% (10%) larger over urban area than rural area. The simulated precipitation is smaller over urban area than rural area during nighttime, probably because of more frequent heavy precipitation in rural area to the north of urban (Fig. 10c). The increase of urban precipitation during daytime is mainly due to the significant thermal effect of urban surface, which induces strong unstable environment over urban area. Consequently, upper-layer atmospheric condition such as the moisture feature is affected. Figure 11c shows the diurnal cycle of atmospheric instability, i.e. lapse rate of potential temperature from surface to 300 m height, in urban and rural area. It can be seen that atmosphere is more unstable over urban area than that over rural area. The

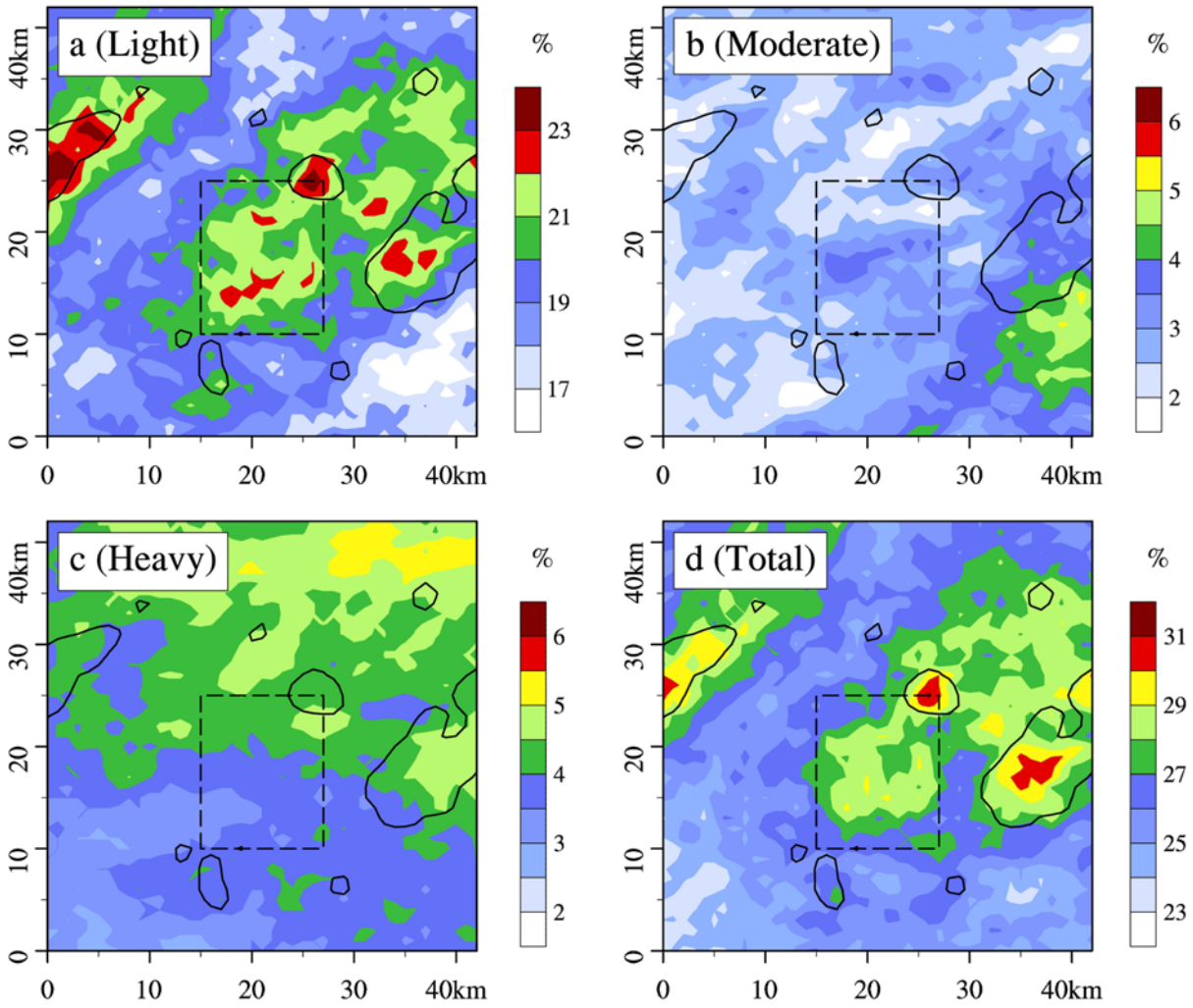

Fig. 10. Simulated spatial distributions of frequency of rain events classified by daily rainfall. Light, moderate, and heavy rain events are defined as those with precipitation rate of 0.2-10 mm d^{-1}, 10-25 mm d^{-1} and > 25 mm d^{-1}, respectively. Black solid and dashed lines denote mountain and urban areas.

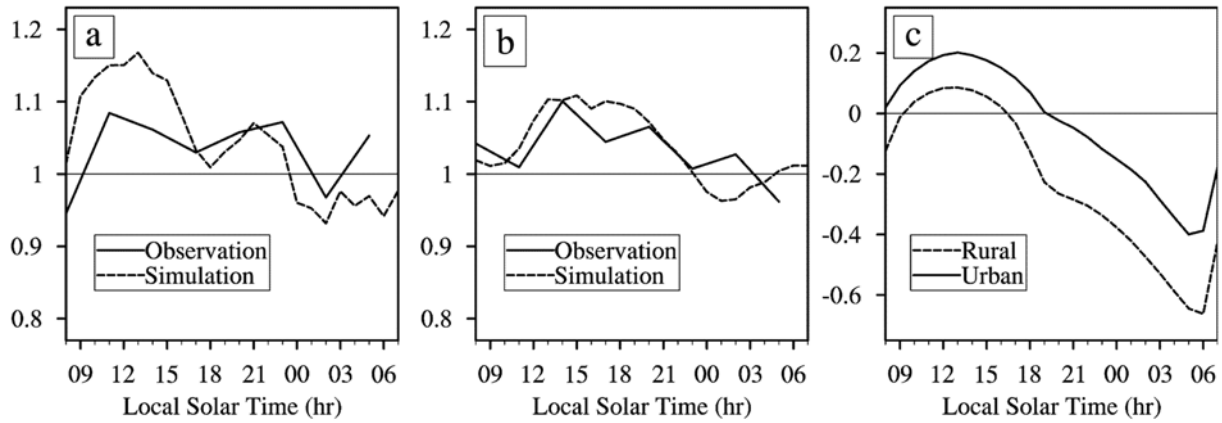

Fig. 11. Observed and simulated diurnal cycles of ratio of urban to rural precipitation for (a) amount and (b) frequency; (c) Simulated diurnal cycles of low-layer instabilities (i.e., lapse rate of potential temperature from surface to 300 m height; unit: K 100 m^{-1}) in urban and rural areas. Urban and rural areas are defined same as in Fig. 7, except that mountain areas are not included in calculating rural precipitation for model results.

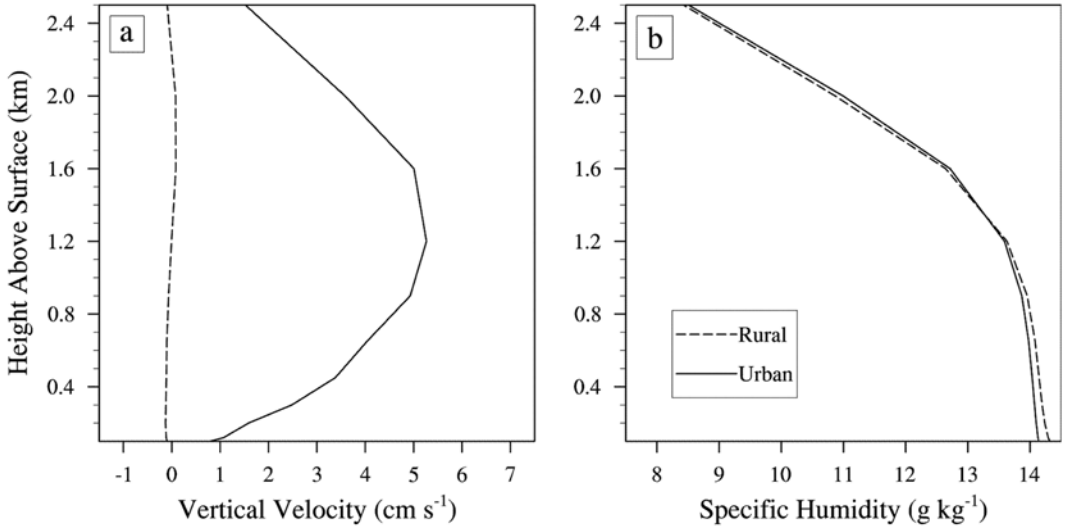

Fig. 12. Simulated vertical distributions of (a) vertical velocity and (b) specific humidity in urban and rural areas at afternoon (12-17 LST). Urban and rural areas are defined same as in Fig. 7.

lapse rate of potential temperature exceeds 0.1 K 100 m^{-1} in urban area from 09 LST to 18 LST. Over rural area, potential temperature lapse rate is below 0.1 K 100 m^{-1}.

Vertical distributions of atmospheric vertical velocity and specific humidity at afternoon (12-17 LST) are shown in Fig. 12. Because of larger atmospheric instability, the maximum upward velocity reaches 5 cm s^{-1} at around 1500 m height above the urban area. The atmospheric vertical motion is very small over rural area. Figure 12b shows that moisture differences between urban and rural area are opposite at low and upper layers, i.e. urban atmosphere is dryer than rural area blow 1500 m, but wetter above 1500 m. The low-layer dry condition over urban area, called as Urban Dry Island, is partially because of strong ascent motion and intense moisture transport vertically from low-layer to upper level. At the same time, moisture can aggregate above 1500 m height, which is very favorable for the formation of precipitation in the afternoon.

To further examine the precipitation distribution in different wind conditions around the city, we classify the wind conditions into 9 categories based on the upper-layer (2 km height) mean wind direction. Because the urban environment becomes unstable rapidly after sunrise (Fig. 11c), the moisture transport before 12 LST may have important effect on the precipitation in the afternoon. Therefore, the wind direction used for the classification is calculated based on the model results from 09 LST to 18 LST. Days with wind speed less than 2 m s^{-1} are defined as weak wind condition. Spatial distributions of afternoon rainfall in each wind classification are presented in Fig. 13. It should be noted that days with wind speed exceeding 15 m s^{-1} are excluded in this analysis because of weak thermal contrast between urban and rural area in very strong wind condition. Considering each wind direction separately can help to detect the urban impact on precipitation in the downwind

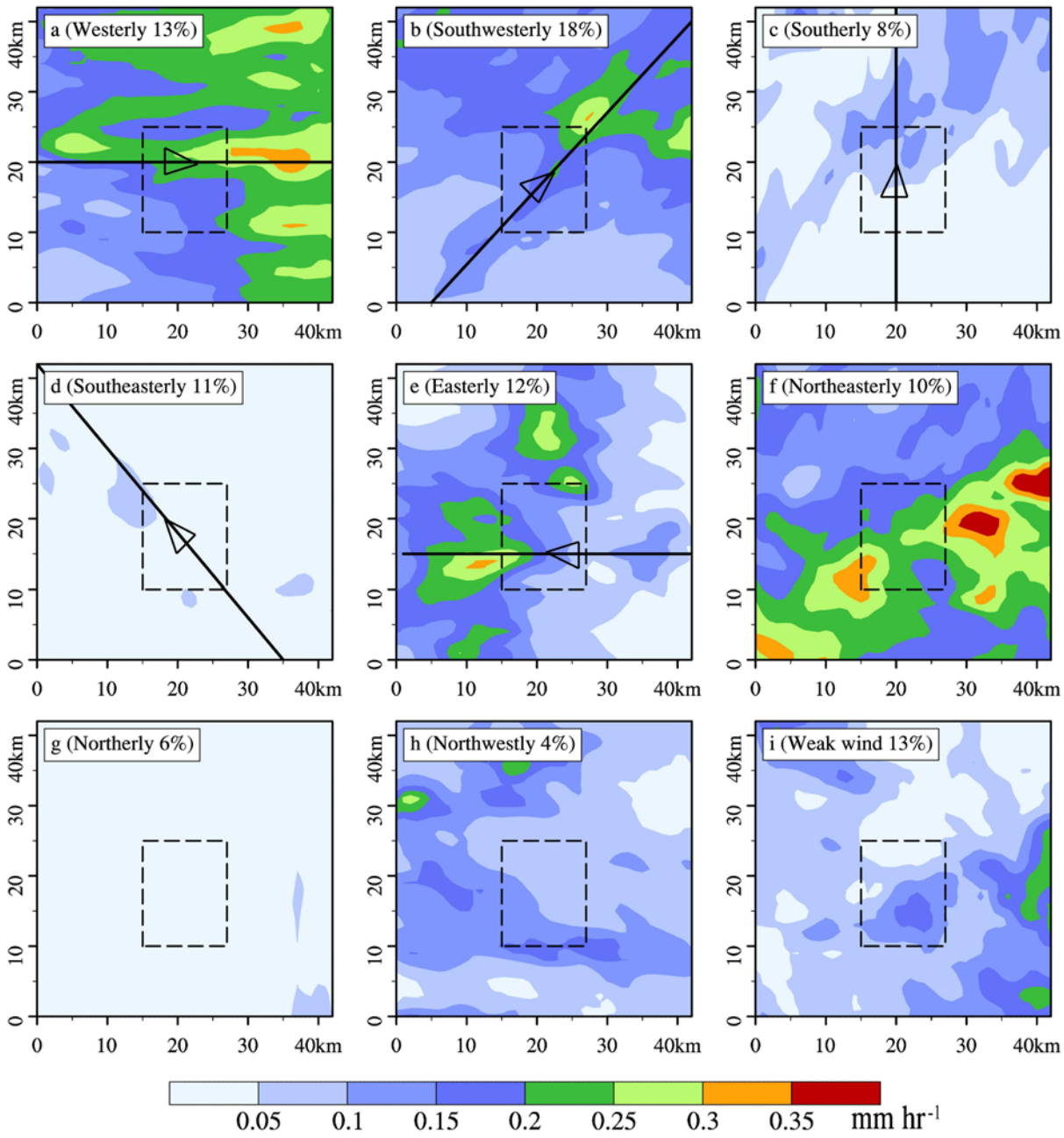

Fig. 13. Simulated spatial distributions of afternoon (12-17 LST) rainfall at different wind directions (2 km height, 09-18 LST). The frequency of occurrences at each wind direction is shown at the top of each figure. Urban areas are marked by dashed lines. Solid lines denote the vertical cross sections used in Fig. 14, with wind directions indicated by arrows.

region. In west wind case (Fig. 13a), a strong rainfall belt is located to the eastern part of urban area and extends to about 15 km downwind. The intensity of the rain belt can reach 0.3 mm hr^{-1}. The precipitation intensity over the upwind urban area is much smaller (i.e., only about 0.1 mm hr^{-1}). Southwest wind is also favorable for the formation of afternoon precipitation. The maximum rainfall center is located to the northeast corner of urban area, with an intensity exceeding 0.25 mm hr^{-1} extending to 10 km downwind. The enhancement of precipitation in the downwind urban area can also be found in other wind conditions (e.g., in days with easterly and northeasterly). For the weak wind condition, we can find that the rainfall center is located inside the urban area. The urban effect on precipitation redistribution is significant, although the spatial distribution of precipitation is mainly controlled by large-scale circulation. Overall the urban underlying surface can effectively enhance the precipitation in the downwind region of urban area.

Above analysis shows the enhancement of precipitation in downwind urban area at afternoon can be reasonably repro-

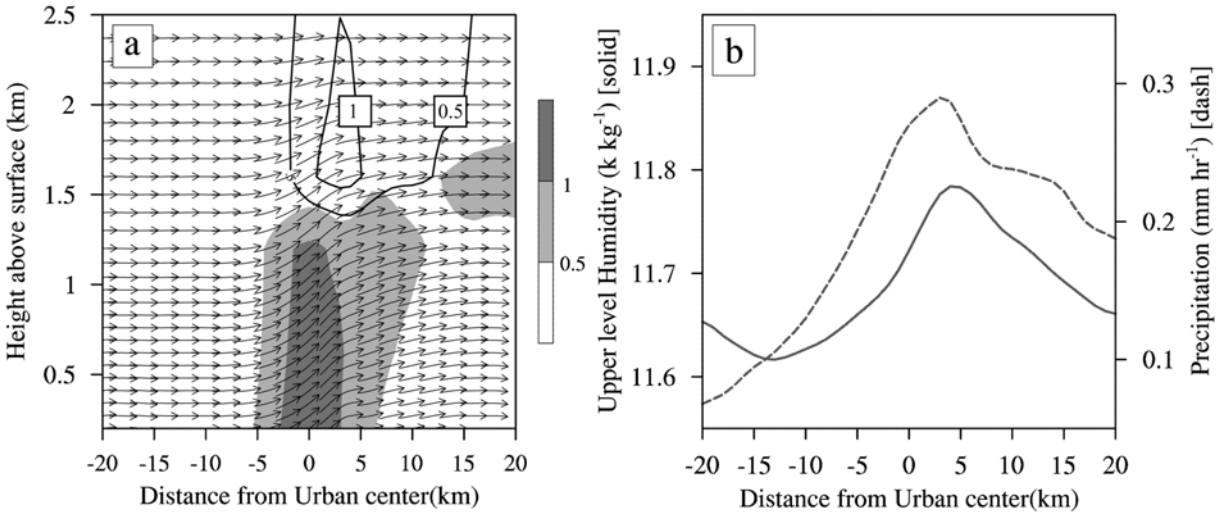

Fig. 14. (a) Alone-wind vertical cross section (averaged from 5 cross sections in Fig. 13, cases with north wind component are not included) of temperature (shade) and humidity (contour) at afternoon (12-17 LST), as well as the in-plane flow vectors; (b) Alone-wind distributions of precipitation and mean-humidity (1.5-2 km above surface) at afternoon. The urban area is nearly from −5 km (upwind) to 5 km (downwind) from urban center. In (a) Temperature and humidity are normalized by the means and variances at each layer.

duced by WRF simulation. The normalized temperature and humidity distribution in the alone-wind vertical cross section is shown in Fig. 14a, which summarize the dynamical mechanism how the warmer urban surface destabilizes the atmosphere and increases the atmospheric moisture at the downwind of city. Figure 14b shows the along-wind distributions of precipitation and upper-layer humidity, from which we can see a close correlation between them along the wind direction. The maximums precipitation and upper-layer humidity are both located about 5 km downwind from urban center. As shown in Figs. 14a and 4b, the upper-layer aggregation of moisture and enhanced upward motion over downwind urban area resulting from surface and low PBL warming increase the downwind precipitation.

5. Conclusion and discussion

In this study, urban climate in Nanjing of eastern China is simulated and examined using a 1-km resolution Weather Research and Forecasting (WRF) model coupled with a single-layer Urban Canopy Model (UCM). We first evaluate the results from fine-resolution model simulations for 10 summers from 2000 to 2009 and find the WRF model is capable of capturing the high-resolution features of urban climate over Nanjing area. Although WRF underestimates the total precipitation amount, the model performs well in simulating the surface air temperature, RH, and precipitation frequency, diurnal cycle and inter-annual variability.

Based on the high-resolution and long-term simulation, we find that extremely hot events occur most frequently in urban area, where the Tmax (Tmin) exceeds 36°C (28°C) in around 40% (32%) of days. UHI effect at surface is more evident during nighttime than daytime, with 20% of cases the UHI intensity larger than 2.5°C at night. However, The UHI affects the vertical structure of PBL more deeply during daytime than nighttime. Net gain for both LH and NR is larger over urban than rural area during daytime. Correspondingly, the net loss of SH and GH at surface are larger over urban area than rural area resulting from warmer skin temperature over the urban surface. Because of different diurnal characteristics of urban-rural differences in LH, GH and other energy fluxes, the near surface UHII exhibits a very complex diurnal feature. We find a negative correlation between UHII and wind speed, with a correlation coefficients of −0.67, suggesting a strong UHI effect at lower-wind speed synoptic condition. We also find the UHI effect is lower under cloudy or rainy days.

Model results reveal a larger precipitation frequency over urban area, mainly contributed by the light rain events (< 10 mm d^{-1}). Consistent with satellite observation, around 10-20% more precipitation occurs in urban area than rural area in the afternoon induced by more unstable urban PBL, which induces a strong vertical atmospheric mixing and moisture transport to the upper layer. A significant enhancement of precipitation is found in the downwind region of urban area in our simulations in the afternoon.

This study applies a high-resolution regional model to conduct a long-term simulation in the Nanjing metropolitan area with a typical monsoon climate regime, aiming to investigate the urban temperature and precipitation effect and their dependence on different synoptic weather conditions, by comprehensively analyzing the land-air energy flux change, low-layer stability, and moisture transport, etc. This kind of research provides some potentially useful insights for better understanding urban climate and its change. However, we only investigate the urban effect by analyzing the high-resolution simulation results in Nanjing area based on the present land

use condition. It will be more ideal to look at the urban effect in future by comparing the simulation results from a series of sensitivity experiments in which past and present land use conditions are incorporated. The uncertainty related to the specific UCM used in this study against other more complex UCMs remains an important issue which deserves further studies. It will be also interesting to include other aspects of urbanization effect, such as the cloud properties and precipitation modifications induced by urban aerosol emission. Besides that, feedback of land-cover and land-use change on large-scale atmospheric circulations is expected to be important as the rapid development of urbanization, which should also be considered in future work.

Acknowledgements. We thank the constructive comment from two anonymous reviewers. This paper is supported by the National Basic Research program of China (2010CB428504). Yun Qian's contribution is sponsored by the U.S. DOE's Office of Science Biological and Environmental Research under a bilateral agreement with the China Ministry of Science and Technology on regional climate research. PNNL is operated for the U.S. DOE by Battelle Memorial Institute under contract DE-AC06-76RLO1830.

REFERENCES

Bornstein, R. D., 1968: Observations of the urban heat island effects in New York City. *J. Appl. Meteorol.*, **7**, 575-582.

Braham, R. R., 1979: Comments on "Urban, topographic and diurnal effects on rainfall in the St. Louis region". *J. Appl. Meteorol.*, **18**, 371-374.

Bukovsky, M. S., and D. J. Karoly, 2009: Precipitation simulations using WRF as a nested regional climate model. *J. Appl. Meteor. Climatol.*, **48**, 2152-2159, doi:10.1175/2009JAMC2186.1.

Burian, S. J., and J. M. Shepherd, 2005: Effects of urbanization on the diurnal rainfall pattern in Houston. *Hydrol. Process*, **19**, 1089-1103.

Changnon, S. A., R. G. Semonin, and F. A. Huff, 1976: A hypothesis for urban rainfall anomalies. *J. Appl. Meteorol.*, **15**, 544-560.

Chen, F., and J. Dudhia, 2001: Coupling an advanced land-surface/ hydrology model with the Penn State/ NCAR MM5 modeling system. Part I: Model description and implementation. *Mon. Wea. Rev.*, **129**, 569-585.

_____, M. Tewari, H. Kusaka, and T. T. Warner, 2006: Current status of urban modeling in the community Weather Research and Forecast (WRF) model. Joint with Sixth Symposium on the Urban Environment and AMS Forum on Managing our Physical and Natural Resources: Successes and Challenges, Atlanta, GA, USA. *Amer. Meteor. Soc.,* CD-ROM. J1.4.

Chin, H.-N. S., M. J. Leach, G. A. Sugiyama, J. M. Leone, H. Walker, J. S. Nasstrom, and M. J. Brown, 2005: Evaluation of an urban canopy parameterization in a mesoscale model using VTMX and URBAN 2000 data. *Mon. Wea. Rev.*, **133**, 2043-2068.

Clarke, J. F., 1969: Nocturnal urban boundary layer over Cincinnati, Ohio. *Mon. Wea. Rev.,* **97**, 582-589.

Coutts, A. M., J. Beringer, and N. J. Tapper, 2007: Impact of increasing urban density on local climate: Spatial and temporal variation in the surface energy balance in Melbourne, Australia. *J. Appl. Meteor. Climatol.*, **46**, 477-493.

Grimmond, C. S. B, and Coauthors, 2010: The International Urban Energy Balance Models Comparison Project: First Results from Phase 1. *J. Appl. Meteor. Climatol.*, **49**, 1268-1292.

_____, and Coauthors, 2011: Initial results from Phase 2 of the international urban energy balance model comparison. *Int. J. Climatol.*, **31**, 244-272.

Hamdi, R., A. Deckmyn, P. Termonia, G. R., Demarée, P. Baguis, S. Vanhuysse, and E. Wolff, 2009: Effects of historical urbanization in the Brussels Capital region on surface air temperature time series: A model study. *J. Appl. Meteor. Climatol.*, **48**, 2181-2196.

Hand, L. M., and J. M. Shepherd, 2009: An investigation of warm-season spatial rainfall variability in Oklahoma City: Possible linkages to urbanization and prevailing wind. *J. Appl. Meteor. Climatol.,* **48**, 251-269.

Holt, T., and J. Pullen, 2007: Urban canopy modeling of the New York City metropolitan area: A comparison and validation of single- and multilayer parameterizations. *Mon. Wea. Rev.*, **135**, 1906-1930.

Hong, S.-Y., and J.-O. J. Lim, 2006: The WRF single-moment 6-class microphysics scheme (WSM6). *J. Korean Meteor. Soc.*, **42**, 129-151.

_____, J. Dudhia, and S.-H. Chen, 2004: A revised approach to ice microphysical processes for the bulk parameterization of clouds and precipitation. *Mon. Wea. Rev.*, **132**, 103-120.

_____, Y. Noh, and J. Dudhia, 2006: A new vertical diffusion package with an explicit treatment of entrainment processes. *Mon. Wea. Rev.*, **134**, 2318-2341.

Huang, L., H. Huang, D. Xiang, J. Zhu, and J. Li, 2007: The diurnal change of air temperature in four types of land cover and urban heat island effect in Nanjing, China (in Chinese). *Ecology and Environment*, **16**, 1411-1420.

Huffman, G. J., and Coauthors, 2007: The TRMM Multisatellite Precipitation Analysis (TMPA): Quasi-global, multiyear, combined-sensor precipitation estimates at fine scales. *J. Hydrometeor.*, **8**, 38-55.

Inoue, T., and F. Kimura, 2004: Urban effects on low-level clouds around the Tokyo metropolitan area on clear summer days. *Geophys. Res. Lett.*, 31, L05103, doi:10.1029/2003GL018908.

Jones, P. D., P. M. Kelly, and C. M. Goodess, 1989: The effect of urban warming on the northern hemisphere temperature average. *J. Climate*, **2**, 285-290.

Kain, J. S., 2004: The Kain-Fritsch convective parameterization: An update. *J. Appl. Meteorol.*, **43**, 170-181.

Khemani, L. T., and B. V. Ramana Murty, 1973: Rainfall variations in an urban industrial region. *J. Appl. Meteorol.*, **12**, 187-194.

Kim, Y.-H., and J.-J. Baik, 2005: Spatial and temporal structure of the urban heat island in Seoul. *J. Appl. Meteorol.*, **44**, 591-605, doi:10.1175/JAM2226.1.

Kusaka, H., and F. Kimura, 2004a: Coupling a single-layer urban canopy model with a simple atmospheric model: Impact on urban heat island simulation for an idealized case. *J. Meteor. Soc. Japan*, **82**, 67-80.

_____, and _____, 2004b: Thermal effects of urban canyon structure on the nocturnal heat island: Numerical experiment using a mesoscale model coupled with an urban canopy model. *J. Appl. Meteorol.*, **43**, 1899-1910.

_____, H. Kondo, Y. Kikegawa, and F. Kimura, 2001: A simple single-layer urban canopy model for atmospheric models: Comparison with multi-layer and slab models. *Bound.-Layer Meteor.*, **101**, 329-358.

_____, F. Kimura, K. Nawata, T. Hanyu, and Y. Miya, 2009: The chink in the armor: Questioning the reliability of conventional sensitivity experiments in determining urban effects on precipitation patterns. proc., 7th International Conference for urban Climate, Yokohama, Japan, Tokyo Institute of Technology, B12-2.

_____, T. Takata, and Y. Takane, 2010: Reproducibility of regional climte in central Japan using the 4-km resolution WRF model. *SOLA*, **6**, 113-116, doi:10.2151/sola.2010-029.

Martilli, A., 2002: Numerical study of urban impact on boundary layer

structure: Sensitivity to wind speed, urban morphology, and rural soil moisture. *J. Appl. Meteorol.*, **41**, 1247-1266.

Masson, V., 2000: A physically-based scheme for the urban energy budget in atmospheric models. *Bound.-Layer Meteor.,* **94**, 357- 397.

Miao, S., F. Chen, M. A. Lemone, M. Tewari, Q. Li, and Y. Wang, 2009: An observational and modeling study of characteristics of urban heat island and boundary layer structures in Beijing. *J. Appl. Meteor. Climatol.*, **48**, 484-501.

Mote, T. L., M. C. Lacke, and J. M. Shepherd, 2007: Radar signatures of the urban effect on precipitation distribution: A case study for Atlanta, Georgia. *Geophys. Res. Lett.*, **34**, L20710, doi:10.1029/2007GL031903.

Oke, T. R., 1981: Canyon geometry and the nocturnal urban heat island: Comparison of scale model and field observations. *Int. J. Climatol.*, **1**, 237-254.

_____, 1982: The energetic basis of the urban heat island. *Quart. J. Roy. Meteor. Soc.*, **108**, 1-24.

Oleson, K. W., G. B. Bonan, J. Feddema, and M. Vertensten, 2008: An urban parameterization for a global climate model. Part II: Sensitivity to input parameters and the simulated urban heat island in offline simulations. *J. Appl. Meteor. Climatol.*, **47**, 1061-1076.

Ren, G., Y. Zhou, Z. Chu, J. Zhou, A. Zhang, J. Guo, and X. Liu, 2008: Urbanization effects on observed surface air temperature trends in north China. *J. Climate*, **21**, 1333-1348.

Roy, S. S., and F. Yuan, 2009: Trends in extreme temperatures in relation to urbanization in the twin cities Metropolitan area, Minnesota. *J. Appl. Meteor. Climatol.*, **48**, 669-679.

Shepherd, J. M., 2005: A review of current investigations of urban-induced rainfall and recommendations for the future. *Earth Interact.,* **9**, 1-27. [Available online at http://EarthInteractions.org.]

Shou, Y.-X., and D.-L. Zhang, 2010: Impact of environment flows on the daytime urban boundary layer structures over the Baltimore metropolitan region. *Atmos. Sci. Lett.*, **11**, 1-6.

Shreffler, J. H., 1978: Detection of centripetal heat-island circulations from tower data in St. Louis. *Bound.-Layer Meteor.*, **15**, 229-242.

Skamarock, W. C., J. B. Klemp, J. Dudhia, D. O.Gill, D. M. Barker, M. G. Duda, X-Y. Huang, W. Wang, and J. G. Powers, 2008: A Description of the Advanced Research WRF Version 3, NCAR Technical Note, NCAR/TN-475+STR, 123 pp.

Souch, C., and S. Grimmond, 2006: Applied climatology: Urban climate. *Prog. Phys. Geog.*, **30**, 270-279.

Tewari M., F. Chen, H. Kusaka, and S. Miao, 2007: Coupled WRF/Unied Noah/urban-canopy modeling system. NCAR WRF Documentation, NCAR, Boulder, 1-22.

Thanh Ca, V., Y. Ashie, and T. Asaeda, 2002: A *k*-ε turbulence closure model for the atmospheric boundary layer including urban canopy. *Bound.-Layer Meteor.*, **102**, 459-490.

Trusilova, K., M. Jung, and G. Churkina, 2009: On climate impacts of a potential expansion of urban land in Europe. *J. Appl. Meteor. Climatol.*, **48**, 1971-1980.

Uno, I., S. Wakamatsu, H. Ueda, and A. Nakamura, 1988: An observational study of the structure of the nocturnal urban boundary layer. *Bound.-Layer Meteor.*, **45**, 59-82.

World Resources Institute, 1996: *World Resources 1996-97: The urban environment*. World Resources Institute, 400 pp. [Available online at http://www.wri.org/publication/world-resources-1996-97-urban-environment.]

Yu, R., T. Zhou, A. Xiong, Y. Zhu, and J. Li, 2007: Diurnal variations of summer precipitation over contiguous China. *Geophys. Res. Lett.*, **34**, L01704, doi:10.1029/2006GL028129.

Zhou, T., R. Yu, H. Chen, A. Dai, Y. Pan, 2008: Summer Precipitation Frequency, Intensity, and Diurnal Cycle over China: A Comparison of Satellite Data with Rain Gauge Observations. *J. Climate*, **21**, 3997-4010.